Defect generation at Si O 2 ∕ Si interfaces by low pressure chemical vapor deposition of silicon nitride

Hao Jin, K. J. Weber, and P. J. Smith

Citation: Applied Physics Letters **89**, 092120 (2006); doi: 10.1063/1.2345247
View online: http://dx.doi.org/10.1063/1.2345247
View Table of Contents: http://scitation.aip.org/content/aip/journal/apl/89/9?ver=pdfcov
Published by the AIP Publishing

Defect generation at SiO_2/Si interfaces by low pressure chemical vapor deposition of silicon nitride

Hao Jin[a] and K. J. Weber
Centre for Sustainable Energy Systems, Faculty of Engineering and Information Technology, The Australian National University, Canberra, Australian Capital Territory 0200, Australia

P. J. Smith
Department of Chemistry, Faculty of Science, The Australian National University, Canberra, Australian Capital Territory 0200, Australia

(Received 11 April 2006; accepted 24 July 2006; published online 1 September 2006)

Low pressure chemical vapor deposition of Si_3N_4 on oxidized Si (111) surfaces causes a change in the properties of the dominant interface defect, the P_b center, observed by electron paramagnetic resonance. The change in the signature of the P_b center is consistent with the formation of an oxynitride layer at the interface, which could be formed during the initial stages of nitride layer deposition. Photoconductivity decay measurements show a concomitant increase in the minority carrier recombination rate at the Si surface. The modified Si surface shows a worse thermal stability than the as-oxidized Si surface. © *2006 American Institute of Physics*. [DOI: 10.1063/1.2345247]

Low pressure chemical vapor deposition (LPCVD) is a reliable batch production method which provides a nearly stoichiometric (Si_3N_4) film. LPCVD Si_3N_4 has a range of properties which make it interesting for photovoltaic applications. It is an excellent diffusion mask[1] and is resistant to chemical attack by alkaline or acidic silicon etchants. In a finished cell, Si_3N_4 provides an excellent antireflection coating.[2] Further, LPCVD Si_3N_4 deposition is highly conformal, allowing even obscured surfaces to be coated uniformly. This is important for some cell structures such as Sliver® cells.[3]

In contrast to plasma-enhanced chemical vapor deposited nitride, LPCVD Si_3N_4 layers do not provide good surface passivation—a key requirement for most photovoltaic applications. Further, the deposition of LPCVD Si_3N_4 directly on Si can lead to irreversible Si bulk damage.[4] For this reason, a thin layer of SiO_2 is usually thermally grown prior to nitride deposition.[4] The $Si-SiO_2$ interface properties post-Si_3N_4-deposition are therefore of great importance, as these properties will determine the recombination properties of the silicon surface in the finished device.

In this letter, we report on a P_b-like defect generated on the oxidized (111) Si surface during LPCVD Si_3N_4 deposition. Quasisteady state photoconductivity decay (QSSPCD) measurements show a concomitant degradation of the surface passivation.

Samples used for electronic paramagnetic resonance (EPR) measurements were *p* type, ~10 Ω cm, (111) Czochralski silicon wafers. Samples were cut with a diamond saw into 25×2.5 mm^2 pieces. They were subsequently etched to remove saw damage from the surfaces. After a standard RCA clean, an oxide layer around 50 nm thick was thermally grown on both sides at 1000 °C (samples A, B, and C). LPCVD Si_3N_4 deposition was done at 775 °C and 0.5 torr, with an ammonia to dichlorosilane flow ratio of 4:1, giving ~50 nm stoichiometric nitride layers on both sides of selected wafers (samples B and C). To prevent interference with the $Si-SiO_2$ interface signal from *K* centers in the nitride layer,[5] the nitride layers for samples B and C were removed in hot phosphoric acid solution without significantly etching the oxide layer. Some of the wafers on which the nitride layer had been removed were oxidized again for 30 min at 1000 °C (samples C). On all EPR samples, a rapid thermal anneal (RTA) was carried out at 800 °C for 3 min in a high flow of nitrogen gas to depassivate the $Si-SiO_2$ interface.[6] A standard RCA clean and de-ionized water rinse were carried out before EPR measurement.

EPR measurements were undertaken using a Bruker 300E spectrometer operating at *X* band (~9.44 GHz), fitted with an Oxford ES-9 liquid helium cryostat with temperature control via an Oxford ITC-4 controller. Measurements were done using a modulation frequency of 100 KHz, modulation amplitude of 5 G, and a microwave power of 20 μW at a temperature of 8.5 K. 20 μW was observed to be nonsaturating. Samples were placed in 3 mm i.d. quartz EPR tubes, which were flushed with pure argon to remove oxygen. The sample tubes were sealed with rubber septa and the sample end was frozen to 77 K. The angle between the sample surface and the magnetic field is within an error of 3°. The P_b center concentration was calculated by double integration of the original signal and comparison with a standard solution signal, obtained under similar conditions.

n-type, ~100 Ω cm (111) and *p*-type, ~100 Ω cm, (100) 550 μm thick float-zoned silicon wafers were used for QSSPCD measurements. After etching in acid solution and a standard RCA clean, samples were phosphorous diffused to form a lightly doped emitter layer (~360 Ω/□ after thermal drive in) on both sides. An oxide around 50 nm thick was thermally grown on both sides, followed by a 30 min forming gas anneal (FGA) (5% H_2 in 95% Ar) at 400 °C. The purpose of phosphorous diffusion and FGA is to achieve a well passivated and hydrogenated Si surface. 50 nm LPCVD Si_3N_4 was deposited on both sides of all samples under the same conditions as for the EPR samples. Selected samples were annealed in nitrogen at 1000 °C. Nitride layers were then carefully removed from the surfaces and a FGA at 400 °C was carried out to ensure a hydrogenated Si surface. Isothermal RTAs at 550 °C and isochronal RTAs for 3 min

[a]Electronic mail: hao.jin@anu.edu.au

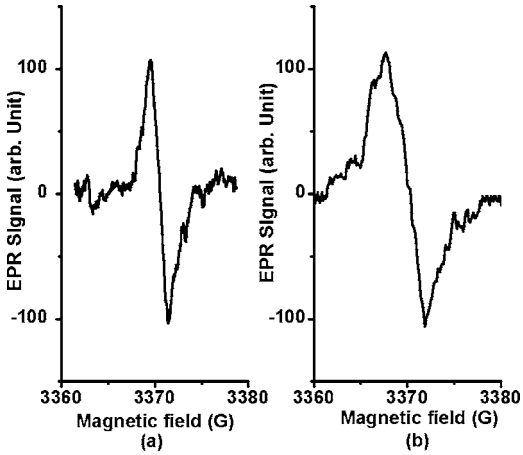

FIG. 1. EPR signals for (a) sample A (as oxidized) and (b) sample B (following nitride deposition and removal) with the magnetic field set parallel to the (111) direction.

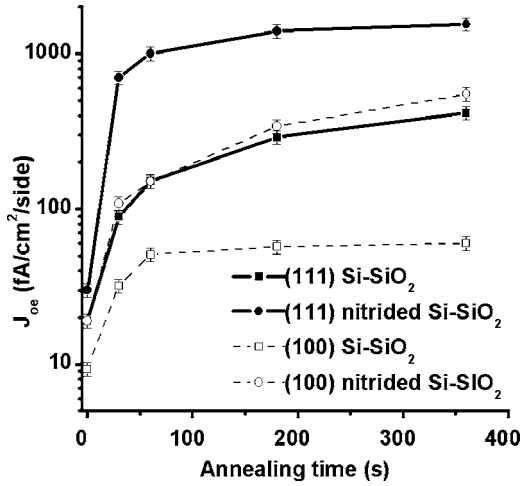

FIG. 2. J_{oe} values after isothermal RTAs at 550 °C. Curves for "Si–SiO_2" are for oxidized samples without nitridation. Curves labeled "post nitride Si–SiO_2" are for oxidized samples with subsequent nitride deposition, nitride strip, and FGA.

were carried out to study and compare the thermal stability of this structure with the thermally grown SiO_2/Si structure.

QSSPCD measurements were used to extract the effective lifetime (τ_{eff}) and surface saturation current density (J_{oe}) from the relationship[7]

$$1/\tau_{eff} = 1/\tau_{hli} + (2J_{oe}n)/(qWn_i^2), \quad (1)$$

where τ_{hli} is the high level injection lifetime of the wafer bulk, n is the photogenerated excess carrier density in the wafer bulk, W is the wafer thickness, n_i is the intrinsic carrier concentration, and q is the electronic charge. Since the phosphorous diffusion and drive in are carried out at a higher temperature (1000 °C) than the subsequent thermal treatments, these thermal treatments do not significantly alter the diffusion profiles. The Si bulk lifetime of all the samples did not degrade significantly during the thermal steps, as indicated by a consistently high effective lifetime (>1 ms) at low injection levels.

Figure 1 displays EPR signals from samples A and B. Table I shows a more detailed comparison between the standard P_b signal from the Si–SiO_2 interface (sample A), the signal from sample B (following nitride deposition and subsequent removal), and reoxidized sample C. The $g_{\|}$ value from sample B is smaller than the standard P_b value (sample A). For sample B, the P_b-like character of the defect is evidenced by the variation of the g value as a function of angle of the magnetic field relative to the (111) direction $g(\theta)$, which is well fitted by the equation

$$g(\theta) = [(g_{\|}\cos(\theta))^2 + (g_{\perp}\sin(\theta))^2]^{1/2}. \quad (2)$$

TABLE I. Comparison of the g value, peak to peak linewidth (ΔB_{pp}), and paramagnetic defect concentration of samples A, B, and C. "$\|$" indicates magnetic field parallel to (111) direction, and "$\perp$" indicates magnetic field perpendicular to (111) direction. The error in the g value is 4×10^{-5}.

	A (as oxidized)	B (nitride deposition and removal)	C (reoxidized)
$g_{\|}$	2.001 41	2.001 25	2.001 35
$\Delta B_{pp\|}$	1.9	4.1	3.6
$g_{\perp}$	2.008 60	2.008 62	2.008 58
$\Delta B_{pp\perp}$	3.8	5.1	4.5
$[P_b]$ (10^{13} cm^{-2})	0.8	1.9	1.0

Reoxidation (sample C) has the effect of increasing the $g_{\|}$ value. The $g_{\perp}$ values for all samples are the same within the limits of experimental error. The ΔB_{pp} at both perpendicular and parallel conditions for sample B is much broader than the standard P_b signal. The paramagnetic defect density more than doubles for sample B and decreases back to near the original level for the reoxidized sample C.

The decrease in $g_{\|}$ and increase of ΔB_{pp} is consistent with the introduction of N atoms into the Si–SiO_2 interface,[8] as a possible by-product result of the LPCVD nitride deposition. Jintsugawa *et al.*[9] have shown that ammonia dissociates at the surface of an oxide layer, leading to the diffusion of N atoms into the oxide. The formation of the oxynitride layer during atmosphoric pressure chemical vapor deposition of silicon nitride on a Si wafer with a native oxide was also observed by Hezel[10] using a combination of Auger electron loss spectroscopy and low energy electron loss spectroscopy. The introduction of Si–N bonds to the ~3 nm thick nonstoichiometric oxide layer near the Si surface generally leads to increased rigidity[8] and more dangling bonds have to be created to release this stress.[11] Another possible explanation for the results is that the changed character and increased density of P_b centers result from the tensile stress[12] introduced by the presence of the nitride layer.

The $g_{\|}$ value and the ΔB_{pp} for the reoxidized sample C is between the value for the standard P_b center and the value for post-nitride-deposition, indicating a gradual change back to standard P_b character during reoxidation.

Figures 2 and 3 show the changes in J_{oe} following isothermal and isochronal RTAs. All J_{oe} values have an error range of 5%–10% due to the measurement accuracy. Figure 2 shows that when no annealing is applied, the changes to the oxide properties resulting from nitride layer deposition cause degradation in the Si surface properties with respect to minority carrier recombination. All values at the no annealing stages (0 min on the graph) come from well hydrogenated surfaces. The trend for (111) and (100) surfaces is similar, although the (111) surfaces display consistently higher values of J_{oe}.

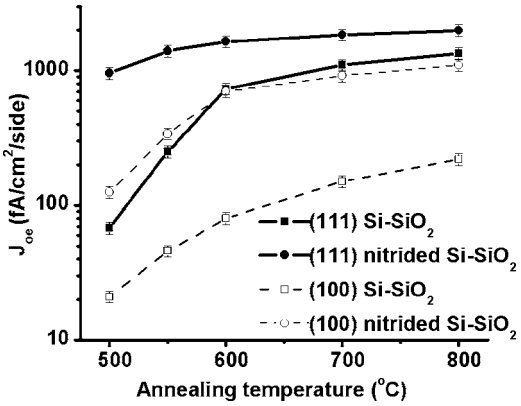

FIG. 3. J_{oe} values after isochronal RTAs for 3 min.

The (111) $Si-SiO_2$ interface displays a more rapid depassivation rate than the (100) interface, probably because the postoxidation annealing generates more interface defects in (111) Si surface than (100) Si surface.[13] For both (100) and (111) samples, the interface following nitride deposition shows a more rapid depassivation rate than the as-oxidized interface, consistent with the increase in interface defects detected by EPR.

In summary, we have found that LPCVD deposition of Si_3N_4 from ammonia and dichlorosilan onto an oxidized silicon surface leads to significant changes in the properties of the $Si-SiO_2$ interface, indicated by a change in the characteristic EPR signature of the P_b center. The changes to the properties and density of the P_b center result in an increase in surface recombination following standard surface passivation treatments and a degradation in the thermal stability of the surface passivation.

The authors would like to thank A. Stesmans of Department of Physics, University of Leuven for many useful advices on EPR operation and discussion on signal analysis and Richard Bramley of Research School of Chemistry, ANU and Ronald Pace of Department of Chemistry, ANU for discussing the EPR operation. Financial support for this project by the Australian Research Council DP0557398 is gratefully acknowledged.

[1]B. Bazin, Solid-State Electron. **15**, 649 (1972).
[2]K. E. Bean, P. S. Gleim, R. L. Yeakley, and W. R. Runyan, J. Electrochem. Soc. **114**, 733 (1967).
[3]K. J. Weber, A. W. Blakers, M. J. Stocks, J. H. Babaei, V. A. Everett, A. J. Neuendorf, and P. J. Verlinden, IEEE Electron Device Lett. **25**, 37 (2004).
[4]M. J. McCann, K. J. Weber, and A. W. Blakers, Prog. Photovoltaics **13**, 195 (2005).
[5]D. Jousse, J. Kanicki, and J. H. Stathis, Appl. Phys. Lett. **54**, 1043 (1989).
[6]P. K. Hurley, B. J. O'Sullivan, F. N. Cubaynes, P. A. Stolk, F. P. Widdershoven, and J. H. Das, J. Electrochem. Soc. **149**, 194 (2002).
[7]D. E. Kane and R. M. Swanson, *Proceedings of the 18th IEEE Photovoltaic Specialists Conference, Las Vegas, NV, 21–26 October 1985* (IEEE, New York, 1985), p. 578.
[8]A. Stesmans and G. Van Gorp, Phys. Rev. B **52**, 8904 (1995).
[9]O. Jintsugawa, M. Sakuraba, T. Matsuura, and J. Murota, Surf. Interface Anal. **34**, 456 (2002).
[10]R. Hezel, Solid-State Electron. **9**, 863 (1981).
[11]A. Stesmans, Phys. Rev. B **48**, 2418 (1993).
[12]Y. G. Jung, A. Pajares, and B. R. Lawna, J. Mater. Res. **19**, 3569 (2004).
[13]A. Stesmans and V. V. Afanas'ev, J. Vac. Sci. Technol. A **16**, 3108 (1998).